

Highly-Efficient, Flexible Piezoelectric PZT Thin Film Nanogenerator on Plastic Substrates

Kwi-Il Park, Jung Hwan Son, Geon-Tae Hwang, Chang Kyu Jeong, Jungho Ryu, Min Koo, Insung Choi, Seung Hyun Lee, Myunghwan Byun, Zhong Lin Wang, and Keon Jae Lee*

Energy harvesters which can convert electrical energy from vibrational and mechanical energy sources are very promising tools to realize the sustainable energy generation in isolated, inaccessible or indoor environments and even in human body conditions.^[1,2] In particular, since the flexible and lightweight energy harvesting device on a single thin plastic substrate can scavenge from the extremely tiny movements such as wind, water flows, heartbeats, diaphragm activities, and respiration movements into electric signals,^[3–5] it can realize not only self-powered flexible electronic systems^[3,4] but also permanent power sources for implantable biomedical devices such as cardiac-tachometers,^[6] pacemakers,^[7] and deep brain stimulators.^[8]

To harvest electrical energy from ambient mechanical energies created by natural sources or from human movements, piezoelectric energy harvesting devices called a nanogenerator (NG) have been proposed and developed by many researchers.^[9–19] Hu et al.^[14] demonstrated densely packed ZnO NWs on the top and bottom surfaces of a plastic substrate in their effort to develop a high-output NG. An energy harvester on a single thin plastic substrate enables high output performance (output voltage of 10 V and output current of 0.6 μA) for operating self-powered wireless data transmission. Piezoelectric polymers such as polyvinylidene fluoride (PVDF) nanofibers have been extensively used to fabricate flexible and stretchable energy harvesting devices due to the soft nature of these polymers.^[15,16] Recently, our group developed nanocomposite-based flexible energy harvesters to achieve scalable, low-cost, and high-output NGs.^[17–19] A piezoelectric nanocomposite was produced by dispersing piezoelectric particles and graphitic

carbons in a polymer matrix which was then sandwiched between the top and bottom electrode-coated plastic substrates.

However, despite their remarkable potential for use as flexible energy harvesters, these above piezoelectric NGs still show either insufficient output performance when used to operate useful mW-level consumer electronics due to their low piezoelectric properties^[14–16] or low energy conversion rates owing to the utilization of two sandwiched plastic substrates or thick piezoelectric polymer layers.^[17–19] In order to enhance the conversion efficiency of NGs, researchers, including our group, have demonstrated an inherently high piezoelectric perovskite thin film on a plastic substrate using a soft-lithographic transfer technique, enabling high-quality thin film materials on a flexible substrate.^[20–23] In those attempts, although highly flexible and sensitive thin film NGs ($\sim 7 \text{ mW} \cdot \text{cm}^{-3}$) were achieved during periodic mechanical deformations, there are still limitations of low output performance ($\sim 1.0 \text{ V}$ and $\sim 26 \text{ nA}$) and complicated process for industrial applications.^[20]

Herein, we demonstrated a large-area PZT thin film on flexible substrates via a laser lift-off (LLO) process and fabricated a thin film NG to realize highly-efficient, lightweight, and flexible piezoelectric energy harvesting devices. The LLO transfer process is a widely commercialized technique that can be used to detach gallium nitride film from a sapphire substrate for a vertical light-emitting diode (LED).^[24–26] We adopt this technique to transfer a high-quality piezoelectric thin film from bulk sapphire substrates to plastic substrates. By XeCl excimer laser irradiation on the backside of the transparent sapphire, the entire area of the PZT thin films can be transferred onto a flexible polyethylene terephthalate (PET) substrate without causing structural damage. The final PZT thin film NG on a single thin plastic substrate converted a high-output performance of $\sim 200 \text{ V}$ and $\sim 150 \mu\text{A} \cdot \text{cm}^{-2}$ from the slight mechanical deformations. The short-circuit current generated from a large-area NG ($3.5 \text{ cm} \times 3.5 \text{ cm}$) reached up to $\sim 8 \mu\text{A}$ and readily allowed more than 100 commercial blue LED arrays to operate during slight bending motions by human fingers.

Figure 1a shows the schematic illustration of the fabrication steps of flexible and large-area PZT thin film NG using the LLO process. An excellent piezoelectric PZT thin film was deposited on a double-side polished sapphire substrate (Hi-Solar Co., $430 \mu\text{m}$ in thickness) by a conventional sol-gel method. A commercially available 0.4 M PZT chemical solution (MEMS solution Co., a 52/48 composition ratio of Zr/Ti with 10 mol% excess PbO) was spin-coated at 2500 rpm for 20 s and subsequently pyrolyzed in air using rapid thermal annealing (RTA) at $450 \text{ }^\circ\text{C}$ for 10 min to remove the organics. These deposition and pyrolysis processes were repeated until a $2 \mu\text{m}$ thick PZT

K.-I. Park, J. H. Son, G.-T. Hwang, C. K. Jeong,
Dr. M. Koo, I. Choi, S. H. Lee, Dr. M. Byun, Prof. K. J. Lee
Department of Materials Science and Engineering
Korea Advanced Institute of Science
and Technology (KAIST)
291 Daehak-ro, Yuseong-gu
Daejeon, 305–701, Republic of Korea
E-mail: keonlee@kaist.ac.kr



Dr. J. Ryu
Functional Ceramics Group
Korea Institute of Materials Science (KIMS)
797 Changwondaero
Seongsan-gu, Changwon
Gyeongnam 642–831, Republic of Korea
Prof. Z. L. Wang
School of Materials Science and Engineering
Georgia Institute of Technology
771 Ferst drive, Atlanta, Georgia 30332–0245, United States

DOI: 10.1002/adma.201305659

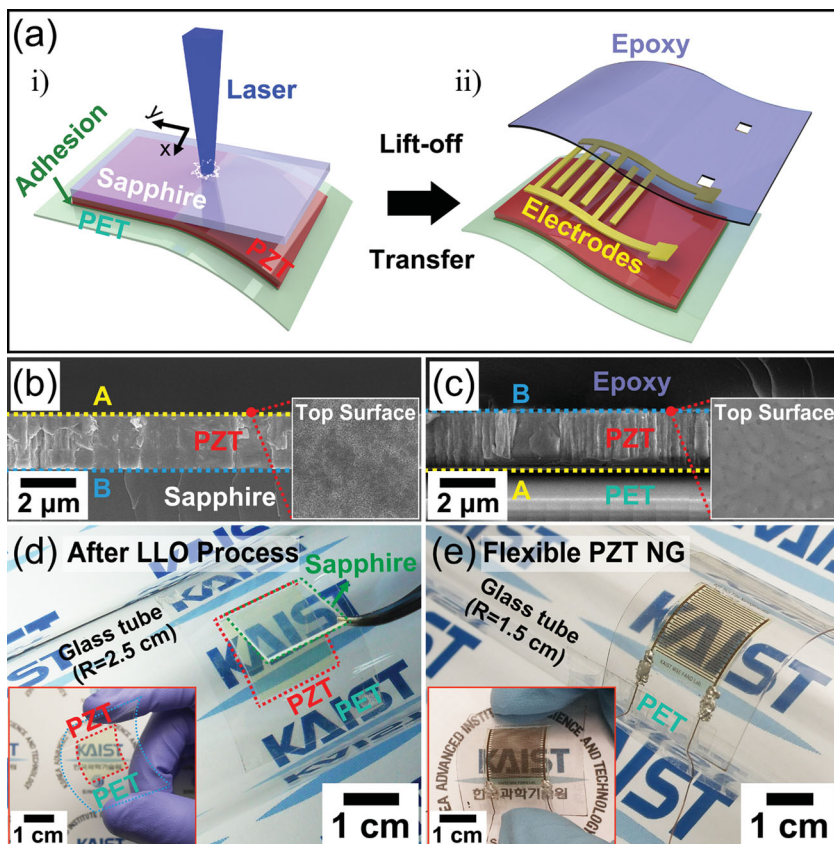


Figure 1. (a) Schematic diagram of the fabrication process for a high-efficient, flexible, and large-area PZT thin film-based NG using the LLO method. By irradiation of a two dimension excimer laser, a 2 μm PZT thin film deposited on a transparent sapphire was successfully transferred onto a flexible PET plastic substrate. Subsequently, the IDEs and protective layer were formed on the PZT thin film to fabricate the NG device. (b,c) The cross-sectional SEM images of PZT thin films on a sapphire (b) and a PET substrate (c). After LLO process, a PZT thin film on an original substrate was inverted at a flexible substrate. The insets show the top surfaces of PZT thin film on sapphire and PET substrates. (d) A PZT thin film (1.5 cm × 1.5 cm) on a PET substrate being detached from a sapphire substrate after LLO process. The inset shows the PZT thin film on a flexible substrate bent by human fingers. (e) The final flexible PZT thin film NG attached to a glass tube and bent by human fingers (the inset).

thin film was obtained after 20 cycles. To crystallize the amorphous film, the PZT thin film was annealed at 650 °C for 45 min in air. The PZT on a sapphire substrate was then placed on a receiver plastic substrate (125 μm PET film, Sigma-Aldrich) coated with ultraviolet (UV) sensitive polyurethane (PU, Norland optical adhesive, No. 73) as an adhesive; then, UV light was used optically to cure the PU layer between the PZT thin film and the PET substrate. To separate the entire area of the PZT thin film layer from the sapphire substrate, a beam spot from a XeCl excimer laser (wavelength of 308 nm) was directed from the backside of sapphire substrates. Because the XeCl laser has a photon energy of 4.03 eV (corresponding to an energy density of 420 mJ·cm⁻²) located between the band gap energies (E_g) of sapphires ($E_g = 10$ eV) and PZT ceramics ($E_g = 3.2\text{--}3.6$ eV), irradiated laser beams can pass through the transparent sapphires and then locally vaporize the interface between the PZT layer and the sapphire substrate, thus separating the PZT thin film on PET substrates from the bulk sapphire mother substrates (corresponding to Figure 1a-i). This LLO transfer process

allows the simple, stable, and large-area transfer of highly-piezoelectric thin films annealed at high temperature onto flexible substrates, which are difficult to handle due to the brittleness of the free-standing ceramic thin film material.^[25–28] Next, interdigitated electrodes (IDEs, 100 nm-thick Au) with a finger length of 1.2 cm, an electrode width of 200 μm, an inter-electrode gap of 100 μm, and 21 finger pairs were deposited onto PZT thin films. To encapsulate the piezoelectric NG device, SU-8 epoxy was coated and then patterned to secure a contact area using a standard photolithography method (corresponding to Figure 1a-ii). Finally, Cu wires were fixed onto metal pads by conductive paste and a poling process was performed at 120 °C by under an applied electric field of 100 kV·cm⁻¹ for approximately 3 hr to enhance the piezoelectric properties (see Supporting Information for details about the fabrication process of the PZT thin film NG, Figures S1a to S1h).

Figures 1b and 1c show cross-sectional scanning electron microscopy (SEM) images of PZT thin films on original (bulk sapphire) and receiver (flexible PET) substrates before and after the LLO process, respectively. During the LLO transfer process, a PZT thin film was flipped over, as clarified by the yellow and blue dotted lines in Figures 1b and 1c, respectively. The insets confirm the absence of cracks or pores on the ‘A’ and ‘B’ surfaces of the PZT thin films. Figure S2a-i in the Supporting Information shows an optical image of PZT thin film on a PET substrate and magnified SEM images of the irradiated areas. Due to the two-dimensional laser beams, there are square spots (500 μm × 500 μm) and overlapped areas

whose SEM images are shown in Figures S2a-ii and S2a-iii. The photograph in Figure 1d shows that the sapphire substrate is being detached from a PZT (1.5 cm × 1.5 cm)/PET substrate (corresponding to Figure 1a-i) after the LLO process; the inset presents the PZT thin film on a flexible substrate bent by human fingers. Figure 1e displays a flexible PZT thin film NG device (corresponding to Figure 1a-ii) attached to a glass tube with a radius of curvature of 1.5 cm. The fabricated PZT thin film NG has not only high flexibility as shown in the inset of Figure 1e but also mechanical stability during bending deformation. These advantages were achieved by the optimized LLO and epoxy passivation processes, resulting in high output performance of thin film NG.

A morphotropic composition (Zr/Ti = 52/48) of PZT ceramics is essential to maximize the energy conversion efficiency.^[29] Moreover, maintaining high-quality piezoelectric properties of PZT thin films onto flexible substrates after a high-temperature LLO transfer process plays a critical role in realizing a high-output flexible energy harvesting device.

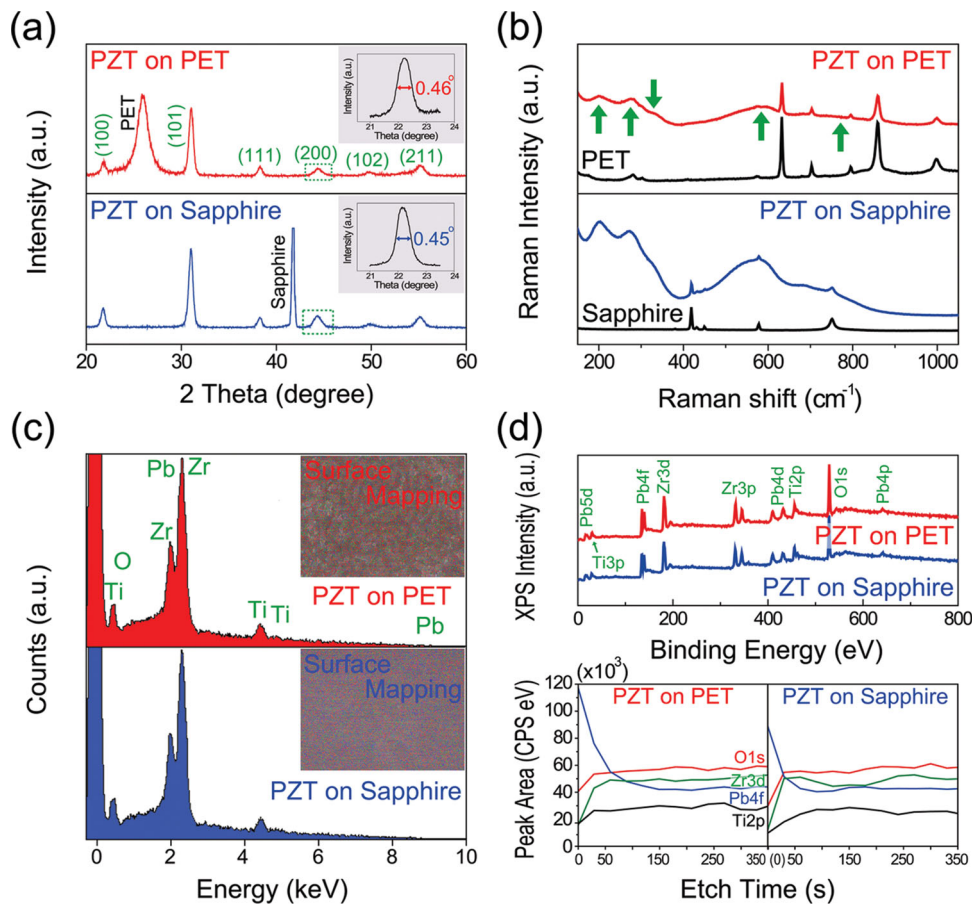


Figure 2. (a) XRD analysis results of PZT thin films on a flexible (top, red) PET and a sapphire (bottom, blue) substrate. The insets indicate the XRD rocking curves of (200) peaks. (b) Raman spectra observed from the PZT thin films before and after LLO process. The peaks indicated by green arrows express the typical results of perovskite PZT. (c) EDS curves obtained from the surfaces of PZT thin films on plastic (top, red) and sapphire (bottom, blue) substrates. The insets show the EDS elemental mapping results. (d) Surface analysis results of PZT surfaces characterized by using XPS. The top graphs show the XPS survey results of PZT thin films before and after LLO process. The bottom graphs present the composition variations at the surface as a function of etching time.

Accordingly, we conducted compositional and structural characterizations of PZT thin films on both sapphire and plastic substrates before and after the LLO process using the X-ray diffraction (XRD), Raman spectroscopy, energy dispersive spectroscopy (EDS) and X-ray photoelectron spectroscopy (XPS). **Figure 2a** shows the XRD analysis results of the PZT thin films on the flexible (top, red) and sapphire (bottom, blue) substrates, elucidating the structural properties before and after the LLO process; PZT thin films on both the bulk and flexible substrates show polycrystallized perovskite structures and the same rocking curve of (200) peak. The peaks indicated by the green arrows of the Raman shift express the typical perovskite PZT phase^[30,31] and have not changed during the LLO process (Figure 2b). Figure S2b presents the Raman spectra of a PZT thin film obtained at selected areas (X, Y, and Z) in Figure S2a-i, indicating that the perovskite PZT phase is maintained despite the surface discrepancy inevitably induced by overlapped laser spots. Figure 2c shows the compositional analysis results of PZT thin films on both sapphire and plastic substrates obtained from EDS elemental mapping of the insets (see Figure S3 for the details of the mapping results and Figure S4 for the EDS

results obtained from the cross-sections of the PZT thin films). The EDS spectrum (bottom of Figure 2c) and chemical composition (Table S1b) of PZT thin films on sapphire substrates were observed not to be substantially different from those (top of Figure 2c and Table S1a) of flexible substrates after the LLO process. Compositional changes of lead (Pb; -0.33%) and zirconium (Zr; -0.44%) was not clearly observed during the instantaneous laser annealing process. We also conducted a surface analysis using XPS to comprehensively characterize the laser-irradiated surfaces of the PZT thin films (Figure 2d). Both the XPS spectra (top panel) of the PZT surfaces and the depth profiles (bottom panel) before and after the LLO process strongly indicate that the elemental binding energy level of the PZT thin films did not change significantly on the surface and even inner side of the PZT. Therefore, we firmly concluded that the conformational transition or structural damage of the PZT thin film was extremely low during the LLO process. This was presumably due to the immediate recrystallization after quenching despite the fact that the interface (PZT layer) between thin film and the sapphire substrate was vaporized or melted by laser irradiation.^[32,33]

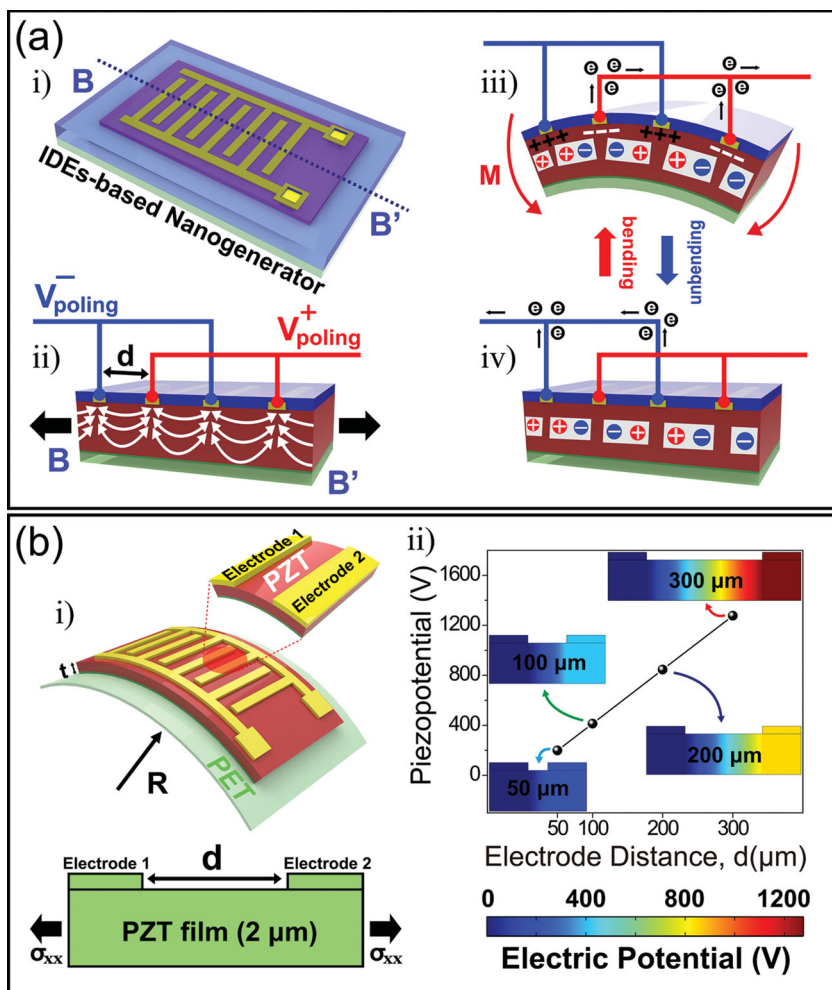


Figure 3. (a) Schematics of the working principle of flexible PZT thin film NG. The dipole direction is parallel to the surface of PZT thin film during the poling process (Figure 3a-ii). By the mechanical bending along the perpendicular direction to IDEs, the positive and negative piezopotentials are generated at neighboring electrodes (Figure 3a-iii), lead to the electron flow and output signals. In the release state (Figure 3a-iv), the piezopotential at each pair of adjacent electrodes disappear and then the electrons move back to original position, generating reverse output signals. (b) Simulation model of an IDEs-based thin film NG (i) and the piezopotential generated inside PZT thin film with different distances between adjacent electrodes (ii).

Figures 3a-i and 3a-ii schematically illustrate the operating mechanism of a PZT thin film NG device. Polycrystalline piezoelectric ceramics can create charge dipoles that are randomly distributed due to the isotropic polarization domains. The directions of these charge dipoles can be modified by applying high electric fields at high temperature in a process known as the poling process, which is an important step when seeking to achieve high-efficiency energy conversion.^[34] Another significant factor in piezoelectricity is the relationship between the applied mechanical stress and the generated charge, defined as a piezoelectric charge constant d_{ij} , where the first i and second j subscripts represent the directions of the poled dipoles and applied force, respectively.^[35–37] In general, polycrystalline piezoelectric materials have five piezoelectric charge constants whose magnitude relationship is as follows: $d_{15} = d_{24} > d_{33} > d_{31} = d_{32}$. Hence, utilizing d_{15} is more effective for high-output energy harvesting

as compared to other constants. However, given that the shear stress-based d_{15} mode is difficult to realize, the d_{31} and d_{33} modes are widely used for piezoelectric applications, in which the two modes are differentiated according to whether the direction of the generated electric signals is perpendicular (d_{31}) or parallel (d_{33}) to the applied stress/strain direction. To demonstrate d_{31} - and d_{33} -types of devices, the top/bottom electrodes and IDEs are commonly used. The open-circuit voltage (V_{3j}) generated when the piezo-materials are deformed by mechanical stress (σ_{xx}) can be expressed as Equation (1),

$$V_{3j} = \sigma_{xx} g_{3j} L_j \quad (1)$$

where g_{3j} is the piezoelectric voltage constant ($g_{3j} = d_{3j}/\epsilon^T$, ϵ^T denotes the permittivity under a constant strain) and L_j is the distance between the electrodes. From Equation (1) above, demonstrating the inter-electrode gap on piezoelectric materials is of critical importance to achieve a high output voltage from a piezoelectric harvester.^[35] For a d_{31} -type device (see Figure S5), L_1 is the thickness (t) of the piezoelectric materials of which scaling up is limited in particular for flexible piezoelectric devices. On the other hand, as shown in (Figure 3a-i), L_3 of the IDEs-based (d_{33} mode) device is the distance (d) between adjacent electrodes; this value can be readily increased to a few hundred micrometers for flexible piezoelectric devices. Furthermore, since the d_{33} and g_{33} constants are approximately twice to triple larger than d_{31} and g_{31} , respectively, IDEs-based harvesters can generate higher outputs compared to metal-piezoelectric (insulator)-metal (MIM)-based devices (d_{31} mode) at similar dimensional scale.^[35–37] Consequently, implementing IDEs as electrodes on a flexible PZT thin film NG device provides a tool for utilizing the piezoelectric d_{33} mode,

thus leading to the realization of a high-output thin film NG.

The working mechanism of an IDE-based NG can be explained by the piezoelectric effect between each pair of adjacent electrodes (Figures 3a-ii to 3a-iv). Once a high temperature and voltage are applied to IDEs deposited on PZT surface, the polarization direction (white arrows) changes depending on the electric fields and consequently becoming parallel to the surface of the PZT thin film (Figure 3a-ii). As shown in Figure 3a-iii, according to the mechanical bending along the direction perpendicular to the IDEs, positive and negative piezopotentials are generated at neighboring electrodes, which is the driving force for the electrons to flow in external load. Subsequently, when the bending stress of the NG is released by unbending motion (Figure 3a-iv), the piezopotential at each pair of adjacent electrodes vanishes and the electrons then move back to their original positions, generating reverse output signals.^[17,18,20]

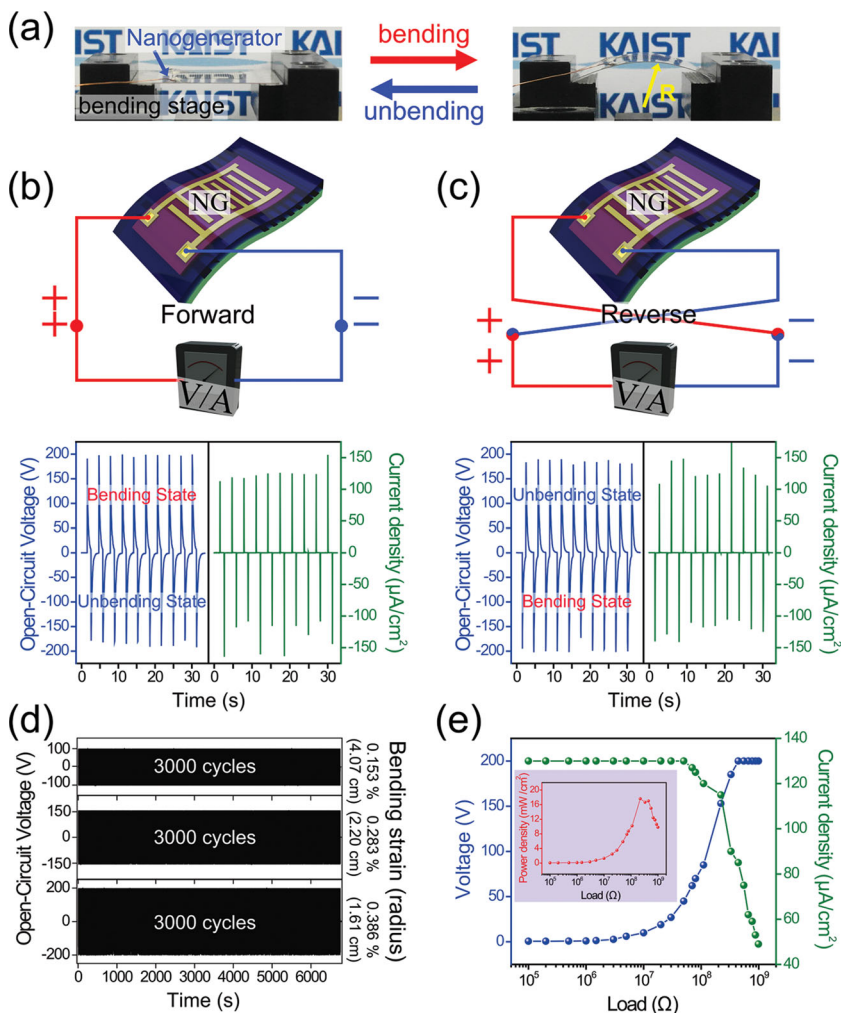


Figure 4. (a) Photographs of PZT thin film NG captured at original (unbending, left) and bending states (right). (b, c) The open-circuit voltage and current density measured from PZT thin film NG in the forward (b) and reverse (c) connections. (d) Strain-dependence and mechanical stability of output voltage generated from PZT thin film NG. The amplitudes of output voltage increase as a function of induced bending strain and show high stability for each 3000 cycles. (e) The measured output voltage and current density under different load resistance varying from 2 k Ω to 1 G Ω . The inset shows the relationship between the output power and external resistance.

To further support the proposed working principle of the IDEs-based thin film NG, we calculated the piezoelectric potential distributions inside the PZT thin film by a finite element analysis (FEA) method using COMSOL software. A simulated model of the device shown in Figure 3b-i was used to simplify an IDEs-deposited PZT thin film NG bent by tensile strain of 0.386% [corresponding to a bending radius (R) of 1.61 cm]. In the case of a piezoelectric thin film on a plastic substrate, a mechanically neutral plane exists inside the plastic substrate, as the film thickness (t) is much thinner compared to the substrate; thus, the thin film was totally deformed by only tensile strain (ϵ) which is nearly equal to the strain of the outer surface of the substrate.^[19,20] From the relationships among the strain, Young's modulus, and stress, the subjected tensile stress of 0.243 GPa can be calculated and employed in the simulated

model (the bottom panel of Figure 3b-i). Figure 3b-ii shows the calculated piezopotential distribution inside a PZT thin film with varying distances between adjacent electrodes. The IDE-based NG can generate a piezopotential difference, which increases linearly with an increasing inter-electrode gap on PZT thin film, while a low piezoelectric difference was calculated in a MIM-based NG (Figure S5). These results are in good agreement with the above mentioned assertions that the output performance can be enhanced by adopting the IDEs approach.

To investigate the energy conversion efficiency of a PZT thin film NG, we measured the output voltage and current signal generated from the device during periodical bending and unbending motions (Figure 4a). Mechanical bending deformation was applied to the device using a linear bending motor with a strain of $\sim 0.386\%$ at a straining rate of $\sim 2.32\% \cdot s^{-1}$. Figure 4b shows the measurement results of the thin film NG (1.5 cm \times 1.5 cm) in the forward connection state, where the open-circuit voltage and the short-circuit current density exceed 200 V and 1.5 μA (corresponding to a current density of 150 $\mu A \cdot cm^{-2}$), respectively, which are much higher than the output performance of previously reported flexible piezoelectric NGs on a single plastic substrate (see Figure S6 for details about the activation area of NG device). In the switching polarity test (Figure 4c), the inverted polarities, negative and positive signals, were sequentially measured by the periodic bending and unbending motions, experimentally proving that the measured signals are generated from the piezoelectric effect of the PZT thin film. We also evaluated the strain-dependent property and mechanical stability of a PZT thin film NG upon the bending and unbending cycles. As shown in the top, center, and bottom panels of Figure 4d, an output voltage of ~ 100 V at bending strain of 0.153% (corresponding to R of 4.07 cm) increases to amplitudes of ~ 160 V and ~ 200 V at a bending strain of 0.283% ($R = 2.20$ cm) and 0.386% ($R = 1.61$ cm), respectively (see Figure S7a for more results measured with varying strains ranging from 0.153% to 0.386%). In addition, the performance of the NG device was observed to be dependent on the angular strain rate at consistent strain (Figure S7b) as well as the input voltage of the poling process (Figure S7c). We also observed that the PZT thin film NG continually produces highly stable output voltages for 9000 bending cycles (Figure 4d); this outstanding working durability benefits from the epoxy passivation process. A fabricated PZT thin film NG without a protective layer shows the electrically or mechanically instability during poling or energy harvesting processes (Figures S8a-i and S8a-ii); these behaviors result in a low output

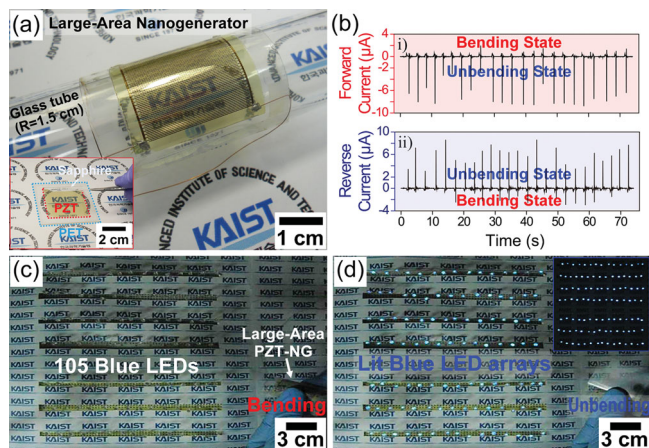


Figure 5. (a) A large-area PZT thin film NG (3.5 cm × 3.5 cm) on a curved glass tube with a radius of 1.5 cm. The inset shows a large-area PZT thin film on PET substrate transferred from a sapphire substrate by LLO process. (b) Current signals measured from a large-area NG irregularly bent by a human finger in forward (top, i) and reverse (bottom, ii) connections. (c) Photograph of the 105 commercial blue LEDs arrayed in series. (d) A snapshot showing the instantaneous lighting up of 105 blue LEDs in series when an NG device was unbent after slight bending by a human finger. The inset shows the driven LED arrays in darkroom.

voltage and current (Figure S8a-iii). On the other hand, in the case of the epoxy-protected NG device (Figures 1e and S8b-i), no cracks were observed on any area of the PZT layer after approximately 10 000 bending/unbending cycles (Figure S8b-ii), leading to higher performance compared to a non-protected device (Figures 4b, 4c, and S8b-iii). To characterize the effective power outputs of the PZT thin film NG, the voltage and current signals were recorded as a function of the external load resistance ranging from 2 kΩ to 1 GΩ (Figure 4e). The instantaneous voltage signals gradually build up as the resistance increase, becoming saturated at a high resistance, whereas the consistent current signals at a low resistance are reduced when the resistance increases. As a result, the instantaneous power density can be calculated by multiplying the output voltage and current, reaching up to 17.5 mW·cm⁻² at a resistance of 200 MΩ, as shown in the inset of Figure 4e.

We demonstrated a large-area PZT thin film NG (3.5 cm × 3.5 cm) and characterized the energy conversion from biomechanical movements, as shown in Figures 5a and 5b. The inset of Figure 5a shows a large-area PZT thin film on a PET substrate (5 cm × 5 cm) transferred from a sapphire substrate. Under irregular and slight bending motions by a human finger, the measured current signals were founded to have a high electric energy of ~8.7 μA (Figure 5b-i) and were also recorded in reverse connection for verifying the measured data, as shown in Figure 5b-ii. The predominance of the output signals by the unbending motions may be due to the discrepancy in the strain rate between the bending/unbending motions inevitably introduced by the human finger. Finally, using this superior self-powered energy source, the 105 commercial LED arrays (forward turn on voltage of ~250 V) aligned in a series were directly powered up without rectifier and charge circuits. The NG device as a power source was reversely connected with the highly bright 105 blue LEDs on handmade circuits and was

then slightly bent by a human finger, as shown in Figure 5c. By unbending motions, the LED arrays were simultaneously turned on, as shown in the captured image of Figure 5d and in the inset (see Supporting Information Video S1 for a video clip showing the 105 blue LEDs being driven when the thin film NG was unbent). These results show that a large-area NG device can serve as a sufficient energy source to operate consumer electronic devices.

In conclusion, we have fabricated a highly-efficient, flexible, lightweight, and large-area piezoelectric PZT thin film NG. By utilizing the LLO process, the entire area of a flexible PZT thin film obtained by a conventional sol-gel method with a subsequent crystallization step at 650 °C was transferred onto a plastic substrate from a sapphire substrate without mechanical damage. The high-output flexible PZT thin film NG was fabricated by employing an IDEs structure with epoxy passivation. During periodical bending/unbending motions, the measured output voltage and current signals reached up to ~200 V and 150 μA·cm⁻², respectively, showing higher output performance than those of the previously reported flexible piezoelectric NGs. The high energy sources harvested from a large-area thin film NG (3.5 cm × 3.5 cm) by irregular human finger motions were used directly to operate over 100 blue LEDs without any external electric source and circuits. Our practical NG technique using the LLO method opens a facile and robust door toward the realization of self-powered flexible electronics and biomedical devices for safety, health, and environmental monitoring system. We are currently investigating the multi-layers stacking or three-dimensional integration to enhance the power density.

Supporting Information

Supporting Information is available from the Wiley Online Library or from the author.

Acknowledgements

This work was supported by the Basic Science Research Program (grant code: NRF-2012R1A2A1A03010415, CAFDC/Keon Jae Lee/No. 2007-0056090) and Center for Integrated Smart Sensors as Global Frontier Project (CISS-2012M3A6A6054187) funded by the Korea government (MSIP) through the National Research Foundation of Korea (NRF). The authors would like to thank KOLON Co., LTD. for their supports.

Received: November 15, 2013

Revised: December 8, 2013

Published online:

- [1] S. P. Beeby, M. J. Tudor, N. M. White, *Meas. Sci. Technol.* **2006**, *17*, R175.
- [2] S. Priya, D. J. Inman, *Energy Harvesting Technologies*, Springer Science, New York, USA **2009**.
- [3] Z. L. Wang, *Nanogenerators for Self-powered Devices and Systems*, Georgia Institute of Technology, Atlanta, USA **2011**.
- [4] Z. L. Wang, W. Z. Wu, *Angew. Chem. Int. Ed.* **2012**, *51*, 11700.
- [5] L. Persano, C. Dagdeviren, Y. W. Su, Y. H. Zhang, S. Girardo, D. Pisignano, Y. G. Huang, J. A. Rogers, *Nat. Commun.* **2013**, DOI: 10.1038/ncomms2639.
- [6] J. Viventi, D. H. Kim, J. D. Moss, Y. S. Kim, J. A. Blanco, N. Annetta, A. Hicks, J. L. Xiao, Y. G. Huang, D. J. Callans, J. A. Rogers, B. Litt, *Sci. Transl. Med.* **2010**, *2*.

- [7] D. H. Kim, N. S. Lu, R. Ghaffari, Y. S. Kim, S. P. Lee, L. Z. Xu, J. A. Wu, R. H. Kim, J. Z. Song, Z. J. Liu, J. Viventi, B. de Graff, B. Elolampi, M. Mansour, M. J. Slepian, S. Hwang, J. D. Moss, S. M. Won, Y. G. Huang, B. Litt, J. A. Rogers, *Nat. Mater.* **2011**, *10*, 316.
- [8] T. I. Kim, J. G. McCall, Y. H. Jung, X. Huang, E. R. Siuda, Y. H. Li, J. Z. Song, Y. M. Song, H. A. Pao, R. H. Kim, C. F. Lu, S. D. Lee, I. S. Song, G. Shin, R. Al-Hasani, S. Kim, M. P. Tan, Y. G. Huang, F. G. Omenetto, J. A. Rogers, M. R. Bruchas, *Science* **2013**, *340*, 211.
- [9] Z. L. Wang, J. H. Song, *Science* **2006**, *312*, 242.
- [10] R. S. Yang, Y. Qin, L. M. Dai, Z. L. Wang, *Nat. Nanotechnol.* **2009**, *4*, 34.
- [11] M. Y. Choi, D. Choi, M. J. Jin, I. Kim, S. H. Kim, J. Y. Choi, S. Y. Lee, J. M. Kim, S. W. Kim, *Adv. Mater.* **2009**, *21*, 2185.
- [12] X. Wang, *Nano Energy* **2012**, *1*, 13.
- [13] Z. L. Wang, G. Zhu, Y. Yang, S. Wang, C. Pan, *Materials Today* **2012**, *15*, 532.
- [14] Y. Hu, Y. Zhang, C. Xu, L. Lin, R. L. Snyder, Z. L. Wang, *Nano Lett.* **2011**, *11*, 2572.
- [15] C. E. Chang, V. H. Tran, J. B. Wang, Y. K. Fuh, L. W. Lin, *Nano Lett.* **2010**, *10*, 726.
- [16] S. Cha, S. M. Kim, H. Kim, J. Ku, J. I. Sohn, Y. J. Park, B. G. Song, M. H. Jung, E. K. Lee, B. L. Choi, J. J. Park, Z. L. Wang, J. M. Kim, K. Kim, *Nano Lett.* **2011**, *11*, 5142.
- [17] K.-I. Park, M. Lee, Y. Liu, S. Moon, G.-T. Hwang, G. Zhu, J. E. Kim, S. O. Kim, D. K. Kim, Z. L. Wang, K. J. Lee, *Adv. Mater.* **2012**, *24*, 2999.
- [18] K.-I. Park, C. K. Jeong, J. Ryu, G.-T. Hwang, K. J. Lee, *Adv. Energy Mater.* **2013**, *3*, 1539.
- [19] S. Y. Xu, Y. W. Yeh, G. Poirier, M. C. McAlpine, R. A. Register, N. Yao, *Nano Lett.* **2013**, *13*, 2393.
- [20] K.-I. Park, S. Xu, Y. Liu, G.-T. Hwang, S. J. L. Kang, Z. L. Wang, K. J. Lee, *Nano Lett.* **2010**, *10*, 4939.
- [21] K.-I. Park, S. Y. Lee, S. Kim, J. Chang, S. J. L. Kang, K. J. Lee, *Electrochem. Solid State Lett.* **2010**, *13*, G57.
- [22] Y. Qi, N. T. Jafferis, K. Lyons, C. M. Lee, H. Ahmad, M. C. McAlpine, *Nano Lett.* **2010**, *10*, 524.
- [23] Y. Qi, J. Kim, T. D. Nguyen, B. Lisko, P. K. Purohit, M. C. McAlpine, *Nano Lett.* **2011**, *11*, 1331.
- [24] M. K. Kelly, O. Ambacher, R. Dimitrov, R. Handschuh, M. Stutzmann, *Phys. Status Solidi. A* **1997**, *159*, R3.
- [25] T. I. Kim, Y. H. Jung, J. Z. Song, D. Kim, Y. H. Li, H. S. Kim, I. S. Song, J. J. Wierer, H. A. Pao, Y. G. Huang, J. A. Rogers, *Small* **2012**, *8*, 1643.
- [26] R. H. Kim, H. Tao, T. I. Kim, Y. H. Zhang, S. Kim, B. Panilaitis, M. M. Yang, D. H. Kim, Y. H. Jung, B. H. Kim, Y. H. Li, Y. G. Huang, F. G. Omenetto, J. A. Rogers, *Small* **2012**, *8*, 2812.
- [27] C. H. Lee, S. J. Kim, Y. Oh, M. Y. Kim, Y. J. Yoon, H. S. Lee, *J. Appl. Phys.* **2010**, *108*.
- [28] Y. H. Do, M. G. Kang, J. S. Kim, C. Y. Kang, S. J. Yoon, *Sens. Actuators B* **2012**, *184*, 124.
- [29] A. J. Moulson, J. M. Herbert, *Electroceramics: Materials, Properties, Applications*, John Wiley & Sons, Chichester, UK **2003**.
- [30] E. R. Camargo, J. Frantti, M. Kakhana, *J. Mater. Chem.* **2001**, *11*, 1875.
- [31] X. Y. Zhang, X. Zhao, C. W. Lai, J. Wang, X. G. Tang, J. Y. Dai, *Appl. Phys. Lett.* **2004**, *85*, 4190.
- [32] K. Y. Li, N. H. Tai, I. N. Lin, *Integrated Ferroelectrics* **2005**, *69*, 135.
- [33] Y. H. Do, W. S. Jung, M. G. Kang, C. Y. Kang, S. J. Yoon, *Sens. Actuators A* **2013**, *200*, 51.
- [34] I. R. Henderson, *Piezoelectric Ceramics: Principles and Applications*, APC International, Pennsylvania, USA **2002**.
- [35] Y. B. Jeon, R. Sood, J. H. Jeong, S. G. Kim, *Sens. Actuators A* **2005**, *122*, 16.
- [36] A. E. Cohen, R. R. Kunz, *Sens. Actuator B* **2000**, *62*, 23.
- [37] E. Choi, S. Q. Lee, T. Y. Kim, K. J. Lee, J. Park, *Proceedings of IEEE 5th International Conference on Nano/Micro Engineered and Molecular Systems*, Xiamen, China, January 20–23 **2010**.